Neurobiology of Aging 34 (2013) 1440–1450

Contents lists available at SciVerse ScienceDirect

Neurobiology of Aging

journal homepage: www.elsevier.com/locate/neuaging

Gray and white matter degeneration revealed by diffusion in an Alzheimer mouse model

Valerio Zerbi [a,b,1], Michiel Kleinnijenhuis [a,c,1], Xiaotian Fang [a], Diane Jansen [a], Andor Veltien [b], Jack Van Asten [b], Nienke Timmer [d], Pieter J. Dederen [a], Amanda J. Kiliaan [a,*,2], Arend Heerschap [b,2]

[a] Department of Anatomy, Donders Institute for Brain, Cognition and Behaviour, Radboud University Nijmegen Medical Centre, Nijmegen, The Netherlands
[b] Department of Radiology, Radboud University Nijmegen Medical Centre, Nijmegen, The Netherlands
[c] Donders Institute for Brain, Cognition and Behaviour, Centre for Cognitive Neuroimaging, Radboud University Nijmegen, Nijmegen, The Netherlands
[d] Department of Neurology, Donders Institute for Brain, Cognition and Behaviour, Radboud Alzheimer Centre, Radboud University Nijmegen Medical Centre, Nijmegen, The Netherlands

ARTICLE INFO

Article history:
Received 4 September 2012
Received in revised form 22 November 2012
Accepted 22 November 2012
Available online 25 December 2012

Keywords:
Alzheimer's disease
Diffusion tensor imaging
Mice
APP/PS1
MRI
White matter
Diffusivity

ABSTRACT

In patients with Alzheimer's disease (AD) the severity of white matter degeneration correlates with the clinical symptoms of the disease. In this study, we performed diffusion-tensor magnetic resonance imaging at ultra-high field in a mouse model for AD ($APP_{swe}/PS1_{dE9}$) in combination with a voxel-based approach and tractography to detect changes in water diffusivity in white and gray matter, because these reflect structural alterations in neural tissue. We found substantial changes in water diffusion parallel and perpendicular to axonal tracts in several white matter regions like corpus callosum and fimbria of the hippocampus, that match with previous findings of axonal disconnection and myelin degradation in AD patients. Moreover, we found a significant increase in diffusivity in specific hippocampal subregions, which is supported by neuronal loss as visualized with Klüver-Barrera staining. This work demonstrates the potential of ultra-high field diffusion-tensor magnetic resonance imaging as a noninvasive modality to describe white and gray matter structural changes in mouse models for neurodegenerative disorders, and provides valuable knowledge to assess future AD prevention strategies in translational research.

1. Introduction

Alzheimer's disease (AD) is the most common type of dementia and is characterized by a progressive loss of neuronal function, leading to gradual memory impairment, confusion, and general withdrawal. Pathologic hallmarks are the accumulation of extracellular amyloid plaques, caused by amyloid-β protein (Aβ) aggregation, and the presence of intracellular neurofibrillary tangles, formed by aggregates of the hyperphosphorylated tau protein. These pathologic changes originate in the medial temporal lobe, especially the entorhinal cortex and hippocampus, spreading further across the limbic cortex and neocortex (Arnold et al., 1991; Braak and Braak, 1995). Along with Aβ- and neurofibrillary tangle gray matter pathology, histological studies identified several changes in white matter structures. More than 50% of confirmed cases of AD show white matter disease in neuropathologic examinations, with a widespread distribution in patients with moderate- to late-stage dementia (Englund and Brun, 1990). Several studies reported a correlation of the incidence of white matter lesions with severity of the underlying AD pathology (Bozzali et al., 2002; Bronge et al., 2002; de Groot et al., 2000). The etiology of AD-related white matter pathology remains to be fully elucidated, although some underlying processes have been proposed, including (1) interhemispheric disconnection through Wallerian degeneration (Tomimoto et al., 2004); (2) axonal damage and gliosis after vascular disease (Englund, 1998); and (3) primary myelin degradation resulting in axonal disconnection (Medina et al., 2006; Xie et al., 2006).

Magnetic resonance imaging (MRI) offers tools to measure white and gray matter architecture in vivo. Diffusion weighted MRI measures the incoherent motion of water molecules for every imaged voxel and provides complementary information to conventional MRI on tissue microstructure (Le Bihan et al., 1986). Since its first description (Basser et al., 1994), diffusion tensor MRI (DT-MRI) has been widely used to investigate white matter because of the relatively coherent organization of axons in fiber bundles that results in

* Corresponding author at: Department of Anatomy, Donders Institute for Brain, Cognition and Behaviour, Radboud University Nijmegen Medical Centre, Geert Grooteplein noord 21, 6525 EZ Nijmegen, The Netherlands. Tel.: +31 24 361 4378; fax: +31 24 361 3789.
E-mail address: a.kiliaan@anat.umcn.nl (A.J. Kiliaan).
[1] Valerio Zerbi and Michiel Kleinnijenhuis contributed equally to this work.
[2] Shared last authorship.

0197-4580/$ – see front matter © 2013 Elsevier Inc. All rights reserved.
http://dx.doi.org/10.1016/j.neurobiolaging.2012.11.017

a marked diffusion anisotropy, with greater diffusivity occurring along the axonal direction. By measurement of the diffusivity in multiple directions, DT-MRI can reconstruct an ellipsoid to model the diffusion in every voxel. The diffusion tensor is characterized by the magnitude of the diffusivity over its 3 axes (eigenvectors). The mean diffusivity (MD) is the average of these diffusivities and captures the size of the tensor. Other informative measures include the axial diffusivity (λ_1) aligned to the primary diffusion direction and the radial diffusivity (RD) that represent the diffusivity perpendicular to this main direction. The shape of the diffusion tensor is often quantified by the fractional anisotropy (FA), which is an index between 0 and 1 that indicates the degree to which diffusivity is different over the 3 axes of the tensor.

DT-MRI is particular well suited for studies of neurological disorders, like AD, because structural changes in neural tissue, like neuronal cell death and white matter microstructural pathology, are reflected in shape and size of the diffusion tensor (Kantarci, 2011). In AD patients changes in DT-MRI parameters are particularly consistent, showing increased diffusivity with loss of directionality—decreased FA—in white matter and increased MD in gray matter regions (Hanyu et al., 1998; Kantarci, 2011; Song et al., 2004). Histologic examinations in brains of AD mice models suggested that myelin loss, decrease in axonal density, and axonal disconnection contribute to the diffusion changes in white matter (Chen et al., 2011; Song et al., 2004). In gray matter, the increased diffusivity has been attributed to neuronal loss, because the diffusivity of water molecules increases when fewer cell membranes restrict their random motion (Sykova et al., 2005). Interestingly, changes in gray matter diffusion (e.g., elevated hippocampal MD) predicted the conversion from mild cognitive impairment to AD similarly or even better than hippocampal volumetric changes in 2 independent studies (Fellgiebel et al., 2006; Kantarci et al., 2005). These results highlight the importance of characterizing the diffusion properties not only in white, but also in gray matter structures, because these contain unique and complementary information about the progression of the disease.

For translational research in AD it is important to perform similar DT-MRI studies in animal models of the disease, but only recently the availability of new dedicated hardware and methods for acquisition and data analysis enabled the study of brain water diffusion in small animals. The results reported in mouse models of cerebral amyloidosis showed white matter diffusion changes similar to those in human studies, but no further investigation on diffusion in gray matter substructures has yet been performed (Song et al., 2004; Sun et al., 2005).

In this study, we aimed to assess water diffusion changes in white and gray matter in a double transgenic mouse model for AD (APP_{swe}/$PS1_{dE9}$) (Jankowsky et al., 2001, 2004). We used state-of-the-art methodology for in vivo DT-MRI data acquisition (Harsan et al., 2010) at ultra-high field (11.7 T) with respiratory and cardiac motion correction and robust tensor estimation (Harsan et al., 2010; Zwiers, 2010). Thereafter, we employed region of interest (ROI)-based and whole-brain voxel-based approaches in combination with tractography algorithm to describe genotype differences with the highest possible spatial resolution. This enables an innovative and accurate description of diffusion changes, for a comprehensive spatial characterization of the underlying pathology in our AD mouse model.

2. Methods

2.1. Animals

The APP_{swe}/$PS1_{dE9}$ founders were obtained from Johns Hopkins University, Baltimore, MD, USA (D. Borchelt and J. Jankowsky, Department of Pathology). A colony was bred and established at the Central Animal Facility at the Radboud University Nijmegen Medical Centre, The Netherlands. The transgenic mice were created by cotransfection with chimeric mouse/human amyloid precursor protein APP_{swe} (mouse APP695 harboring a human Aβ domain and mutations K595N and M596L linked to Swedish familial AD pedigrees) and human presenilin 1 with deletion of exon 9 ($PS1_{dE9}$) vectors controlled by independent mouse prion protein promoter element (Jankowsky et al., 2001, 2004). These 2 genes cointegrate and cosegregate as a single locus. Breeder mice were backcrossed to C57BL6/J for 12 generations to obtain the animals for this study. Throughout the duration of the experiment the mice were housed in groups. Room temperature was kept at 21 °C with an artificial 12-hour light:dark cycle. Food and water were available ad libitum. The experiments were performed according to Dutch federal regulations for animal protection and were approved by the Veterinary Authority of the Radboud University Nijmegen Medical Centre.

2.2. Magnetic resonance imaging

Twelve-month-old male APP_{swe}/$PS1_{dE9}$ transgenic mice ($n = 9$) and age-matched wild type (WT) littermates (C57BL6/J $n = 15$) were used for DT-MRI. Isoflurane (3.5% for induction and approximately 2% for maintenance) was used for anesthesia. The anesthetic concentration was adjusted during the experiment in order to maintain the breathing frequency at 65–85 per minute. The mice were placed in a stereotactic device to immobilize the head. Body temperature was measured using a rectal thermometer and maintained at 37 °C using a heated air flow device.

Magnetic resonance (MR) measurements were performed on a 11.7 T BioSpec Avance III small animal MR system (Bruker BioSpin, Ettlingen, Germany) equipped with an actively shielded gradient set of 600 mT/m. We used a circular polarized volume resonator for signal transmission and an actively decoupled mouse brain quadrature surface coil for signal reception (Bruker BioSpin).

Gradient echo images in the axial, sagittal, and coronal orientation were acquired to visualize the anatomy and the morphology of the mouse brain structures. Imaging parameters were: echo time = 5 ms, repetition time = 630 ms, flip angle = 12°, field of view = 40 × 40 mm, matrix size = 512 × 512, slice thickness = 0.345 mm.

Diffusion MRI was performed following a modified protocol of Harsan et al. (2010). In short, 31 axial slices covering the whole brain were acquired with a spin-echo planar imaging protocol. B0 shift compensation, navigator echoes, and automatic ghost correction algorithm were implemented to limit the occurrence of ghosts and artifacts. Encoding b-factors of 0 s/mm^2 (b0 images; 5×) and 1000 s/mm^2 were used, and diffusion-sensitizing gradients were applied along 30 noncollinear directions of 3-dimensional space. Other imaging parameters were: echo time = 21.4 ms, repetition time = 7750 ms, time between the application of diffusion gradient pulses $\Delta = 10$ ms, diffusion gradient duration $\delta = 4$ ms, number of segments = 4, total resolution 156 × 156 × 500 μm. This results in a total scan time of 18 minutes for each mouse.

2.3. Data preprocessing

For spatial normalization, a study-specific template was created of all WT and transgenic animals using Advanced Normalization Tools (ANTs. V1.9.x, http://picsl.upenn.edu/ANTS/). A group-wise normalization procedure (SyGN, as implemented in the buildtemplateparallel.sh script V0.0.13) was employed on the realigned mean diffusion image of each mouse (Avants et al., 2008). The default implementation was followed with 4 iterations using mutual information as the initial affine similarity metric and cross-correlation as 'greedy SyN' diffeomorphic transformation metric. A mask that included the entire brain was manually defined in the

normalized coordinate space and transformed to each animal's native space for use in subsequent processing.

The diffusion tensor was estimated for every voxel using the PATCH algorithm (Zwiers, 2010). This method incorporates realignment and is robust against regional (e.g., cardiac motion) and slice-wise (e.g., bulk motion) artifacts by providing a weight for every voxel that reflects the probability of being an outlier in the tensor fitting. From the eigenvalues of the diffusion tensor, the rotationally invariant indices FA, MD, RD, and λ_1 were calculated. The resulting volumes were spatially normalized to the template space using the affine parameters and deformation field obtained at template creation.

2.4. Voxel-based group comparison

Regional differences in spatially normalized FA, MD, RD, and λ_1 maps between $APP_{swe}/PS1_{dE9}$ mice and WT littermates were assessed voxel-wise using MATLAB R2008a (Mathworks, Natick, MA, USA) and Statistical Parametric Mapping 5 (SPM5, Wellcome Department of Clinical Neurology, London, UK) with the SPMMouse toolbox (Sawiak et al., 2009). Two *t* tests were performed to identify increase ($APP_{swe}/PS1_{dE9} > WT$) or decrease ($APP_{swe}/PS1_{dE9} < WT$) genotype-wise differences in the framework of the general linear model. Statistical significance for an individual voxel was established at $p < 0.01$, uncorrected for multiple comparisons. The locations of significant voxels exceeding a minimum cluster size of 4 (to achieve cluster size approximately 0.05 mm^3 as in Dubois et al. (2008) were determined with an anatomical atlas (Franklin and Paxinos, 1997). The contrasts were then color coded and overlaid onto images derived from the template image.

2.5. ROI-based group comparison

To compare our results with other studies, the diffusion-tensor imaging (DTI) parameter maps FA, MD, RD, and λ_1 were evaluated for significant genotype differences with a ROI approach. For the ROI-based approach, 10 white matter tracts were selected bilaterally across the mouse brain based on the atlas of (Franklin and Paxinos, 1997). These regions include the anterior commissure, anterior commissure posterior, and genu—body—splenium of the corpus callosum (cc), cerebral peduncle, external capsule, fimbria of the hippocampus, fornix, and optic tract. The hippocampus and cerebral cortex (all cortical areas above the cc) were also defined approximately at −1.22 up to −2.54 posterior to bregma.

2.6. Image analysis and tractography

To determine the fiber systems involved in areas of significant difference between $APP_{swe}/PS1_{dE9}$ and WT, we investigated those regions with tractography. We used MRtrix' (v.0.2.9) constrained spherical deconvolution with spherical harmonic order 4, for obtaining fiber orientation distributions (Tournier et al., 2007). Deterministic constrained spherical deconvolution tractography was initiated from the voxel-based analysis (VBA) clusters of significant FA differences separately for $APP_{swe}/PS1_{dE9} > WT$ and $APP_{swe}/PS1_{dE9} < WT$. Fibers were seeded from these regions until 10,000 fibers with a minimum of 1 mm, maximum length of 20 mm, and step size 0.02 mm. Termination criteria were set at: FA threshold < 0.1 and curvature radius > 0.05.

2.7. Histology

To compare the axonal organization in hippocampal and cortical gray matter structures with our DT-MRI images and to demonstrate the correlation between changes in water diffusion as found with DT-MRI and the degeneration of the brain tissue, we performed 2 staining methods: 1 for myelin and nerve cell bodies (Klüver-Barrera staining) and 1 for myelinated and unmyelinated nerve fibers (Bodian silver staining). These stainings were performed on brain tissue of 2 $APP_{swe}/PS1_{dE9}$ and 2 WT littermates of the scanned group of mice. After perfusion with saline the brains were removed from the skull and immersion fixated overnight in 4% phosphate buffered paraformaldehyde. After fixation, the brain tissue was dehydrated in alcohol series, cleared in xylene and embedded in paraffin. Sections of 5 μm were cut on a rotary microtome, mounted on albumen-coated glass slides and dried overnight at 37 °C. After removing the paraffin by xylene the sections were rehydrated in alcohol series and rinsed in distilled water. The brain sections (bregma −2.92 mm, based on the atlas of Franklin and Paxinos, 1997) were stained according to Bodian (1936, 1937), or according to Klüver and Barrera (1953). After dehydration in alcohol series, sections were cleared with xylol and mounted in Entellan.

2.8. Statistical analysis

Statistical analyses for the ROI-based approach were performed using SPSS v16.0 (SPSS Inc, Chicago, IL, USA). Results are expressed as mean ± standard deviation (SD). Differences between genotypes in multiple ROIs were analyzed with multivariate analysis of variance with Bonferroni correction. Statistical significance was established at $p < 0.05$.

3. Results

For each mouse, FA, MD, RD, and λ_1 maps were generated from the DT-MRI data (Fig. 1a). The high resolution of the images enabled us to recognize the organization of many structures in the mouse brain. This is illustrated in Fig. 1b for 10 slices of color-coded FA maps of a WT mouse, overlaid with the primary diffusion direction λ_1. These composite images incorporate in each voxel information from the anisotropy degree and the main diffusion orientation, and help to identify several white matter substructures that are difficult to distinguish by other image modalities (Jiang and Johnson, 2010). For example, neighboring white matter structures like the cerebral peduncle and the optic tract are readily discriminated from these images (Fig. 1b). Other white and gray matter structures are also easily identifiable, like the anterior commissure anterior, anterior commissure posterior, genu—body—splenium of the cc, external capsule (ec), fimbria of the hippocampus, and fornix.

3.1. Voxel-based analysis and tractography

An anatomic template was overlaid with *p*-value maps (*p*-value with threshold at 0.01, minimum voxel cluster size set at 0.05 mm^3) to visualize the distribution of water diffusivity differences between the $APP_{swe}/PS1_{dE9}$ transgenic and WT mouse brains. Voxels that differ significantly are indicated by the colored overlay (Fig. 2). RD, MD, λ_1, and FA were investigated using this method.

The VBA indicates several areas of significant differences between the 2 genotypes. In several clusters in the cc and ec, a decrease in all DT-MRI parameters (FA, MD, RD, and λ_1) was visible. The decrease in FA resulted from the stronger decrease in λ_1 than in RD. In the fimbria of the hippocampus, bilateral clusters of voxels showed a large increase in MD, RD, and λ_1, with decreased FA.

In the area corresponding to the cerebral peduncles, a decrease in RD is notable, together with an increase in FA and a slight decrease in λ_1. Similar changes were detected in other areas, like the internal capsule and the lateral posterior thalamus nuclei.

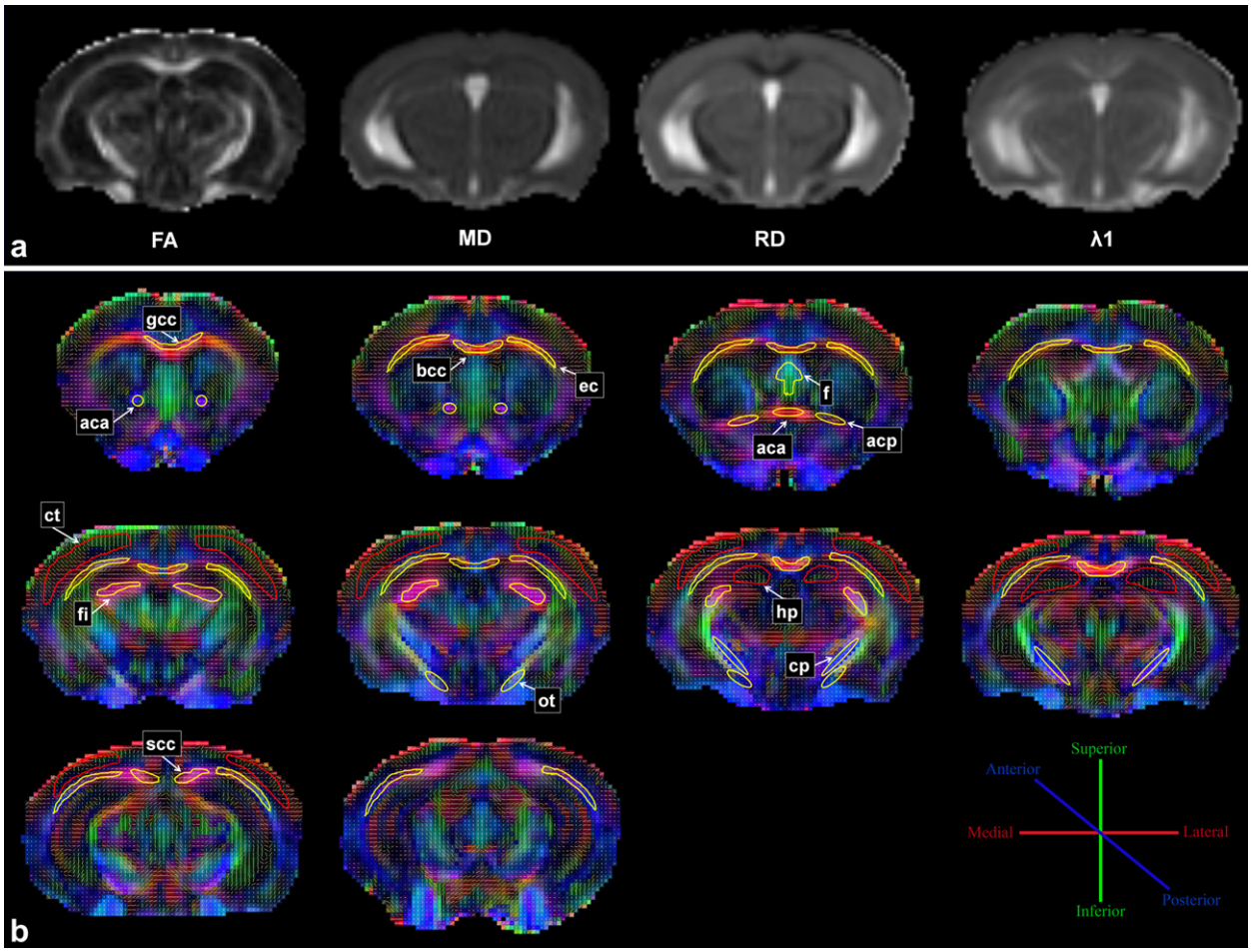

Fig. 1. Coronal images of diffusion parameter maps from a wild type mouse. Fractional anisotropy (FA), mean diffusivity (MD), radial diffusivity (RD), and axial diffusivity (λ1) maps are shown (a). Regions of interest were selected on a representative series of FA maps, color-coded by the diffusion orientation, overlaid with the primary diffusion direction λ_1 (b). Anterior commissure anterior (aca), anterior commissure posterior (acp), cerebral peduncle (cp), optic tract (ot), genu (gcc)—body (bcc)—splenium of the corpus callosum (scc), external capsule (ec), fimbria of the hippocampus (fi), fornix (f), hippocampus (hc), and cerebral cortex (ct) were defined approximately from bregma 1.10 mm to −3.16 mm, based on the atlas of Franklin and Paxinos (1997).

The fiber tracts of a WT mouse shown in Fig. 3 were obtained from seeding fibers in the clusters of significant differences in FA from the VBA (overlaid in the pictures). The seeded voxels were differentiated in areas where $APP_{swe}/PS1_{dE9}$ mice showed lower FA values (Fig. 3a, in blue) and higher FA values (Fig. 3b, in red) compared with WT. By tracking fibers from voxels of significantly lower FA in the $APP_{swe}/PS1_{dE9}$ mice, we identified several white matter fiber bundles involved in degeneration processes in these mice. Among them, the whole corpus callosum with its extensions into in the cortex and the fimbria of the hippocampus were the areas most affected (Fig. 3a). Conversely, the tracts resulting from seed voxels of higher FA in the transgenic mice did not form single coherent fiber bundles, but these voxels showed a marked colocalization with crossing fibers, originating from the thalamus, midbrain, and hypothalamus (Fig. 3b).

Interestingly, the VBA indicated clusters of significant genotype differences located in gray matter structures. In left and right hippocampus, the MD, RD, and λ_1 increased in transgenic mice compared with the control (Fig. 2). The FA did not change significantly. A closer look at these results shows that most of the differences are present in the lacunosum moleculare layer (LMol) and in the molecular layer of dentate gyrus (Mol) layers of the hippocampus (Fig. 2). In some cortical areas, mainly in the visual cortex, a few clusters of decreased FA and λ_1 were also found.

3.2. ROI-based analysis

For a quantitative assessment of genotype differences, we analyzed the DT-MRI indices in ROIs drawn on several white and 2 gray matter structures. The results are shown in Table 1. A significant decrease in diffusion along the main fiber orientation (λ_1) was seen in the anterior commissure posterior ($p = 0.030$), cerebral peduncle ($p = 0.020$), body of cc ($p = 0.010$), and fornix ($p = 0.025$) of transgenic mice. In the latter 3 regions, this was also associated with a decreased MD ($p = 0.004$, $p = 0.044$, and $p = 0.023$, respectively). In the fimbria of the hippocampus, we found a strong increase in RD ($p < 0.001$), linked with a decreased FA ($p = 0.013$) and increased MD ($p = 0.037$). In the total hippocampal area, we detected a strong significant increase in MD, RD, and λ_1 ($p = 0.001$, $p = 0.003$, and $p = 0.002$, respectively). In the cerebral cortex, a decrease in FA was seen ($p = 0.035$). Overall, diffusion values resemble the results from other similar studies (Harsan et al., 2010; Ruest et al., 2011).

3.3. Gray matter diffusion and genotype comparison with histology

To illustrate the advantage of high resolution MR imaging to assess directional diffusivity in gray matter structures, magnifications of the DT-MRI images of hippocampal area (Fig. 4) and cortical

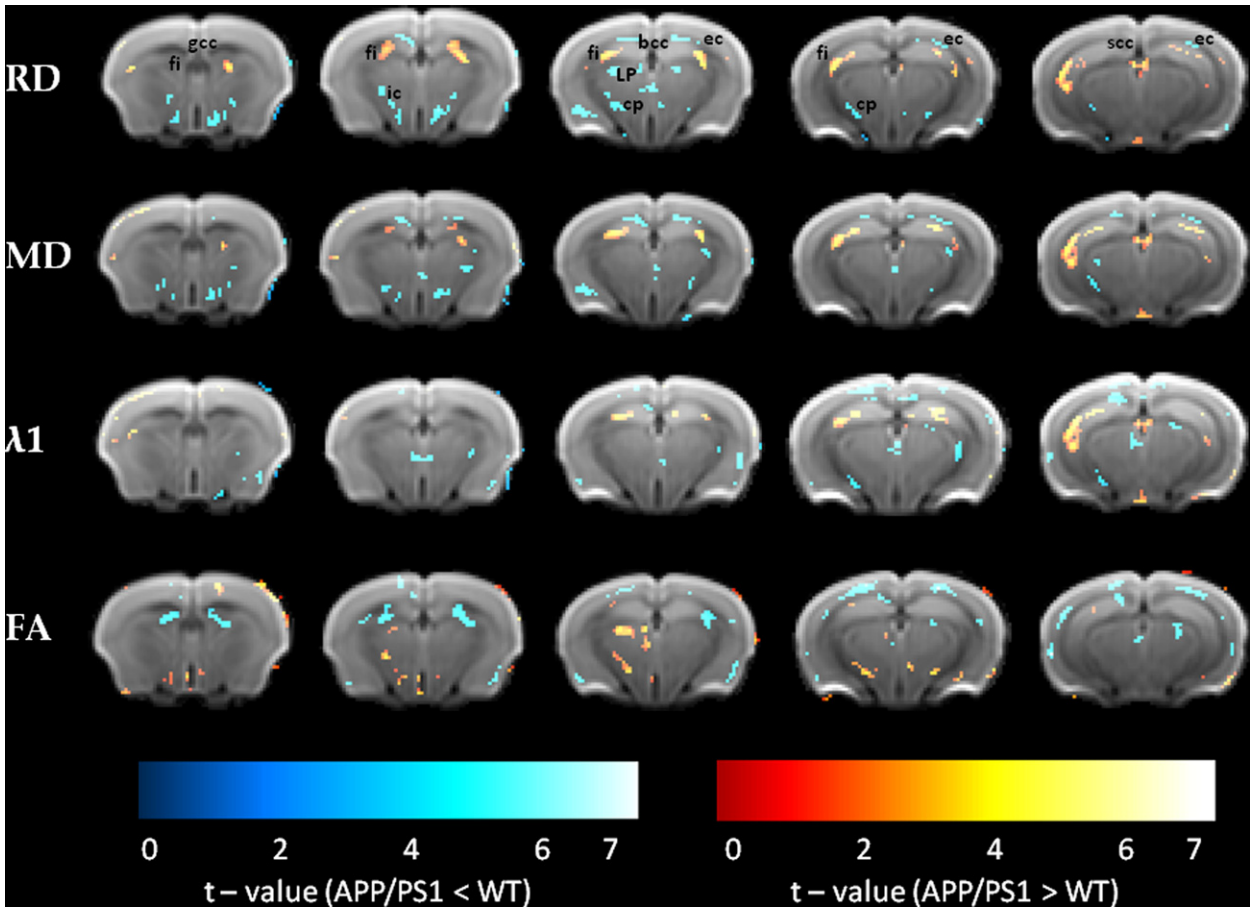

Fig. 2. Voxel-based analysis indicate significant differences in radial diffusivity (RD), mean diffusivity (MD), axial diffusivity (λ_1), and fractional anisotropy (FA) in transgenic $APP_{swe}/PS1_{dE9}$ mouse brains compared with wild type. Five rostral to caudal axial diffusion weighted maps are overlaid with voxels that showed a significant difference ($p < 0.01$, voxel cluster size 0.05 mm^3). The voxel color indicates a negative or positive change in the transgenic mice compared with the wild type mice. VBA results were overlaid on top of a template image derived from the dataset. A widespread increase in RD is found in the hippocampus and in the fimbria (fi), and decreases are present in the corpus callosum (cc), cerebral peduncle (cp), and in the lateral posterior thalamus nuclei (LP). The MD decrease is found among others in the internal capsule (ic) and in the cc. An increased MD in the hippocampus and fi is also present. An increase in λ_1 is found along the boundaries of the hippocampus, and a decrease is present in the splenium of cc (scc). FA reduction was observed in areas such as the scc, fi, and cortex. Increases in FA are found in the cp, ic, and LP.

area (Fig. 5) were compared with stainings for myelin and nerve cells (Klüver-Barrera) and staining for nerve fibers (Bodian). The anatomical layers which constitute the hippocampus are discernible by the different orientation of their diffusion tensors (Fig. 4a and b): 2 layers of marked anisotropy and medial-lateral orientation, correspond to the stratum radiatum and the Mol, and they alternate with 2 thin layers of more isotropic diffusion: for example, the LMol and the granular layer of the dentate gyrus (GrDG)/polymorph layer of the dentate gyrus.

The actual orientation of the axons is visualized in the hippocampal layers by the Klüver-Barrera staining (Fig. 4c and d) and by the Bodian staining (Fig. 4e). In the latter, the alignment of the fibers in the direction radial to the cortical surface is discernible in the stratum radiatum and in the Mol layers. An incoherent alignment of the nerve fibers is found instead in the LMol, GrDG, and polymorph layer of the dentate gyrus. Overall, a good anatomic agreement is found between DT-MRI data and nerve fibers directionality and alignment.

Sections of the same bregma (−2.92 mm) stained according to Klüver-Barrera, are shown to demonstrate neurodegeneration in the $APP_{swe}/PS1_{dE9}$ (Fig. 4d) compared with WT mice (Fig. 4c).

In the $APP_{swe}/PS1_{dE9}$, the GrDG layer is significantly thinner compared with WT mice because of a marked reduction of neurons as shown with the Klüver-Barrera staining (Fig. 4d, arrows). In the magnification insert of the $APP_{swe}/PS1_{dE9}$ mouse (Fig. 4g) a decreased amount of stained healthy neuronal cell bodies is visible in this layer and many more pycnotic dark stained cells are shown compared with the WT (Fig. 4f), suggesting degenerated neurons. Spherical-shaped areas with no staining are present in the $APP_{swe}/PS1_{dE9}$ tissue, most likely related to the presence of Aβ plaque deposits (Fig. 4d, asterisks). No major differences in amount of nerve fibers between $APP_{swe}/PS1_{dE9}$ and WT mice were detectable with the Bodian staining (not shown).

In the cerebral cortex the primary diffusion direction radial to the cortical surface can be clearly identified (Fig. 5). This corresponds well with the axonal orientation, as shown with Klüver-Barrera and Bodian staining of the same areas (Fig. 5c–e respectively). Comparing $APP_{swe}/PS1_{dE9}$ (Fig. 5d) and WT mice (Fig. 5e), the only noticeable difference in the cortical tissue was the loss of both neurons and fibers in regions that are likely related to presence of the Aβ plaques (Fig. 5d, asterisks).

4. Discussion

DT-MRI has become accepted in clinical practice as preferred tool for quantitative assessment of the structural integrity of white matter and, to some extent, of gray matter (Basser et al., 1994; Beaulieu, 2002). Nowadays, it is possible to apply water diffusion

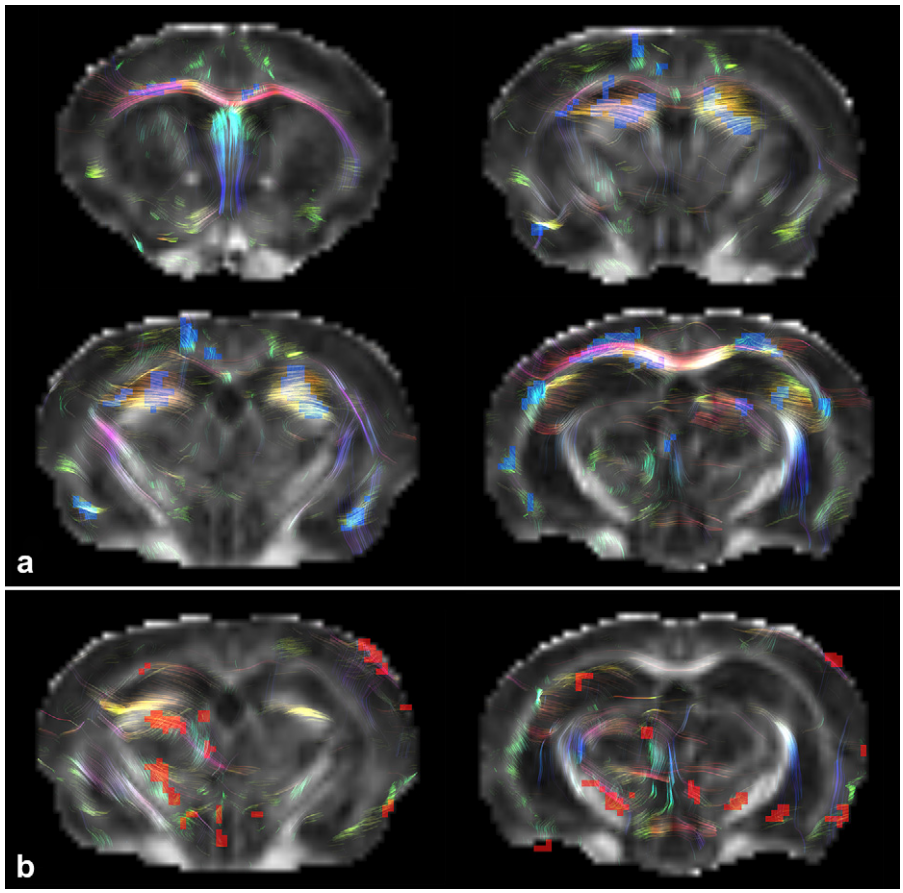

Fig. 3. Example of fiber tracts of a wild type mouse seeded from the clusters of significant differences in fractional anisotropy (FA). (a) Tracts from the voxels where $APP_{swe}/PS1_{dE9}$ mice showed significantly lower FA values (overlaid as blue voxels). The tracts defined in (a) suggest the areas that appear to be more affected in transgenic mice, particularly corpus callosum, fimbria of hippocampus, and fornix. (b) shows Tracts from clusters where APP mice showed significantly higher FA values (overlaid as red voxels). The tracts in (b) spread out in multiple directions, suggesting the presence of crossing fibers.

MRI also in translational research and acquire high-resolution DTI images of the mouse brain in vivo (Harsan et al., 2010). A recent study in rat brain validated the correlation between DTI parameters and microstructural tissue properties (Budde and Frank, 2012). This is of particular interest in experimental AD research to monitor white and gray matter degeneration in AD models for the investigation of new preventive strategies. A reduction of the apparent diffusion coefficient was found in neocortical areas of 25-month-old APP23 transgenic mice, which was associated with fibrillar amyloid deposits and glial proliferation (Mueggler et al., 2004). In DT-MRI studies, changes in FA and λ_1 were found in 15-month-old PDAPP mice and 12-month-old Tg2576 mice in some white matter areas, including cc and external capsule, followed by an increase in RD as the pathology progressed (Song et al., 2004; Sun et al., 2005). Remarkably, the same effects were not seen in an ex vivo study with APP_{swe} mice brains, likely because of fixation-related alterations in postmortem analysis (Harms et al., 2006).

In this study, we aimed for a comprehensive analysis of the DT-MRI changes occurring not only in white but also in gray matter in 12-month-old $APP_{swe}/PS1_{dE9}$ mice in vivo. At 12 months of age these transgenic mice already exhibit widespread parenchymal deposits of Aβ in several cortical and subcortical regions, together with progressive Aβ accumulation in the vascular walls, leading to cerebral amyloid angiopathy (Garcia-Alloza et al., 2006; Jankowsky et al., 2004). Furthermore, deficits in learning and memory tasks were described at this age in the Morris water maze test, indicating an initial decline of neuronal function (Malm et al., 2011).

4.1. White matter

A histologic characterization of white matter degeneration of 24-month-old APP/PS1 mice (with the Swedish KM670/671NL, and London mutation V717I introduced in human sequence APP751 × HMG PS1 M146L) has been recently reported (Chen et al., 2011). This study demonstrated fiber tract volume reduction, loss of axonal neurofilaments, and myelin breakdown in axonal bundles of the cc and the anterior commissure. Interestingly, atrophy of the cc is also classically observed in AD patients (Teipel et al., 2002). Our DT-MRI results describe in vivo changes in white matter diffusion that resemble the fiber tract anomalies reported by Chen et al., including changes in the cc. Compared with WT littermates, the $APP_{swe}/PS1_{dE9}$ mice display a smaller and more isotropic diffusion ellipsoid in some areas of the cc, particularly in the body of cc, with the largest reduction occurring in the direction of the fiber bundles (λ_1). This situation has been associated with a Wallerian-like degeneration in the presence of axonal disconnection and volume reduction of fiber tracts, because the water molecules have more restricted diffusion mostly along the tracts (Sun et al., 2008). Wallerian-like degeneration and processes of retrogenesis are also described in the cc of mild AD patients (Di Paola et al., 2010). We did not find an increase in RD in the cc, that has been linked to myelin degradation of the axonal bundles (Song et al., 2005), but contrarily we found a minor decrease. This same trend has been shown by Sun et al., in 12-month-old Tg2576 mice. In their experiment, mice were measured at multiple time points, and the increase in RD in the cc

Table 1
Diffusion tensor parameters of the regions of interest

Structure	APP/PS1	Wild type	*p*
Anterior commissure			
RD	0.51 ± 0.03	0.50 ± 0.05	n.s.
MD	0.69 ± 0.03	0.70 ± 0.04	n.s.
λ1	1.06 ± 0.08	1.08 ± 0.05	n.s.
FA	0.45 ± 0.05	0.46 ± 0.06	n.s.
Anterior commissure posterior			
RD	0.62 ± 0.08	0.65 ± 0.02	n.s.
MD	0.74 ± 0.06	0.77 ± 0.02	n.s.
λ1	0.99 ± 0.04	1.02 ± 0.03	0.030
FA	0.31 ± 0.11	0.28 ± 0.02	n.s.
Cerebral peduncle			
RD	0.42 ± 0.03	0.44 ± 0.03	n.s.
MD	0.70 ± 0.02	0.74 ± 0.02	0.004
λ1	1.27 ± 0.08	1.33 ± 0.04	0.020
FA	0.61 ± 0.04	0.60 ± 0.02	n.s.
Corpus callosum - Body			
RD	0.61 ± 0.05	0.64 ± 0.03	n.s.
MD	0.74 ± 0.05	0.78 ± 0.03	0.044
λ1	0.99 ± 0.06	1.06 ± 0.04	0.01
FA	0.37 ± 0.04	0.39 ± 0.03	n.s.
Corpus callosum - Genu			
RD	0.64 ± 0.08	0.59 ± 0.06	n.s.
MD	0.82 ± 0.09	0.80 ± 0.05	n.s.
λ1	1.18 ± 0.16	1.22 ± 0.05	n.s.
FA	0.39 ± 0.06	0.44 ± 0.05	0.058
Corpus callosum - Splenium			
RD	0.73 ± 0.11	0.79 ± 0.11	n.s.
MD	0.97 ± 0.09	1.03 ± 0.11	n.s.
λ1	1.47 ± 0.09	1.52 ± 0.12	n.s.
FA	0.44 ± 0.08	0.41 ± 0.04	n.s.
External capsule			
RD	0.71 ± 0.07	0.69 ± 0.03	n.s.
MD	0.83 ± 0.06	0.81 ± 0.02	n.s.
λ1	1.06 ± 0.07	1.06 ± 0.02	n.s.
FA	0.29 ± 0.03	0.30 ± 0.02	n.s.
Fimbria of the hippocampus			
RD	0.78 ± 0.08	0.65 ± 0.04	0.000
MD	1.05 ± 0.09	0.96 ± 0.08	0.037
λ1	1.60 ± 0.19	1.58 ± 0.18	n.s.
FA	0.45 ± 0.07	0.51 ± 0.05	0.013
Fornix			
RD	0.40 ± 0.04	0.42 ± 0.07	n.s.
MD	0.64 ± 0.06	0.70 ± 0.05	0.023
λ1	1.10 ± 0.18	1.60 ± 0.11	0.025
FA	0.55 ± 0.08	0.59 ± 0.08	n.s
Optic tract			
RD	0.55 ± 0.06	0.54 ± 0.03	n.s.
MD	0.76 ± 0.06	0.77 ± 0.03	n.s.
λ1	1.20 ± 0.10	1.24 ± 0.04	n.s.
FA	0.48 ± 0.06	0.50 ± 0.03	n.s.
Hippocampus			
RD	0.80 ± 0.05	0,75 ± 0.02	0.003
MD	0.87 ± 005	0.81 ± 0.02	0.001
λ1	1.01 ± 0.06	0.94 ± 0.02	0.002
FA	0.16 ± 0.03	0.16 ± 0.03	n.s.
Cerebral cortex			
RD	0.70 ± 0.02	0.70 ± 0.02	n.s.
MD	0.77 ± 0.02	0.77 ± 0.02	n.s.
λ1	0.89 ± 0.02	0.91 ± 0.02	n.s.
FA	0.16 ± 0.02	0.18 ± 0.02	0.035

Data are given as (mean ± SD). Statistical analysis for genotype differences was performed between $APP_{swe}/PS1_{dE9}$ transgenic mice ($n = 9$) and age-matched wild type littermates (C57BL6/J, $n = 15$) using a region of interest-based approach. The mean (MD), radial (RD), and axial (λ_1) diffusivities are expressed in units of 10^{-3} mm^2/s.
Key: FA, fractional anisotropy; n.s., nonsignificant.

was detected only after 16 months of age (Sun et al., 2005). Together these findings indicate that myelin degradation in the cc occurs in an advanced stage of the pathology. This corresponds with histologic findings, in which volume reduction of the cc in APP/PS1 mice—at 24 months of age—appeared to be largely caused by atrophy of fiber bundles, loss of axonal neurofilaments, and only partly by myelin breakdown (Chen et al., 2011). In our staining on myelin and nerve fibers, we could not detect well-defined differences in cc between $APP_{swe}/PS1_{dE9}$ and WT mice. However, the lack of staining in some areas of the cc and the external capsule in the transgenic mice are likely related to deposits of Aβ, which could interfere with the shape and the integrity of the axonal bundles (Sun et al., 2005). The presence of Aβ in white matter regions of $APP_{swe}/PS1_{dE9}$ mice already has been reported at this age by ex vivo histopathologic studies (Zerbi et al., 2012). Contrary to what we expected, the VBA showed also regions of colocalized increased FA and decreased RD in the $APP_{swe}/PS1_{dE9}$, (e.g., in the cerebral peduncles and thalamic areas below the hippocampus). This would suggest that in these regions WT mice and not $APP_{swe}/PS1_{dE9}$ mice show signs of white matter pathology and myelin degradation. However, as highlighted by our tractography images, in these regions the white matter is not coherently aligned as in the cc, ec, or anterior commissure (ac), and crossing fibers are frequent. The FA in such regions is naturally lower than would be the case in any 1 of these bundles separately. In the depicted thalamic regions, the higher FA and lower RD that we found in $APP_{swe}/PS1_{dE9}$ mice could therefore be caused by a degeneration of 1 fiber tract, in voxels that normally include more fibers with different orientations. This event would cause 1 fiber group to dominate in the diffusion quantification, resulting in a voxel with higher FA and lower RD. This concept has been discussed recently for AD patients, in whom the increase of FA in crossing-fiber areas was associated with early white matter alterations (Douaud et al., 2011). A recent study on stained rat brain slices further demonstrated that these regions are likely to include multiple fiber populations (Budde and Frank, 2012).

4.2. Gray matter

The interpretation of the data from gray matter diffusion imaging requires distinct considerations. Whereas the white matter consists of relatively coherent bundles of myelinated axons, in gray matter regions like cortex or hippocampus, the constituents are far more heterogeneous in size, shape, and orientation. The larger volume fraction of cell bodies of neurons and glial cells compared with white matter fiber bundles yield an increased isotropic diffusion. Because the dendrites are only partially coherently organized and the axons are not homogeneously distributed and might be myelinated or unmyelinated, their contribution to the diffusion signal is uncertain and might vary in different substrate regions. Hence, if the analysis of FA do not account for these contributions, it might lose its descriptive meaning. Instead, other parameters like the averaged diffusivity along all the diffusion directions (MD) are considered more informative. There is growing evidence that the increased MD in the hippocampus is associated with loss of neurons and can be used as a good predictor of AD progression (Carlesimo et al., 2010; Fellgiebel et al., 2006; Kantarci et al., 2005). In the present study, a marked increase in MD was seen in the hippocampus of $APP_{swe}/PS1_{dE9}$ mice, suggesting neurodegeneration. With the increased spatial sensitivity of the VBA, we were able to further circumscribe these changes to the LMol and the Mol. To the best of our knowledge, this is the first study that reports diffusion changes in AD models in specific subregions of the hippocampus, which is a key area in AD pathogenesis, related to spatial memory and learning and among the earliest and most severely affected regions in AD pathology in these mice (Braak and Braak, 1991; Garcia-Alloza et al., 2006).

The increase of MD in gray matter has been described in several human AD studies, and is often explained to be caused by neuronal degeneration and cell loss, resulting in less hindered water diffusion (Fellgiebel et al., 2004). Although reports about neuronal loss in mice expressing amyloid precursor protein mutations are

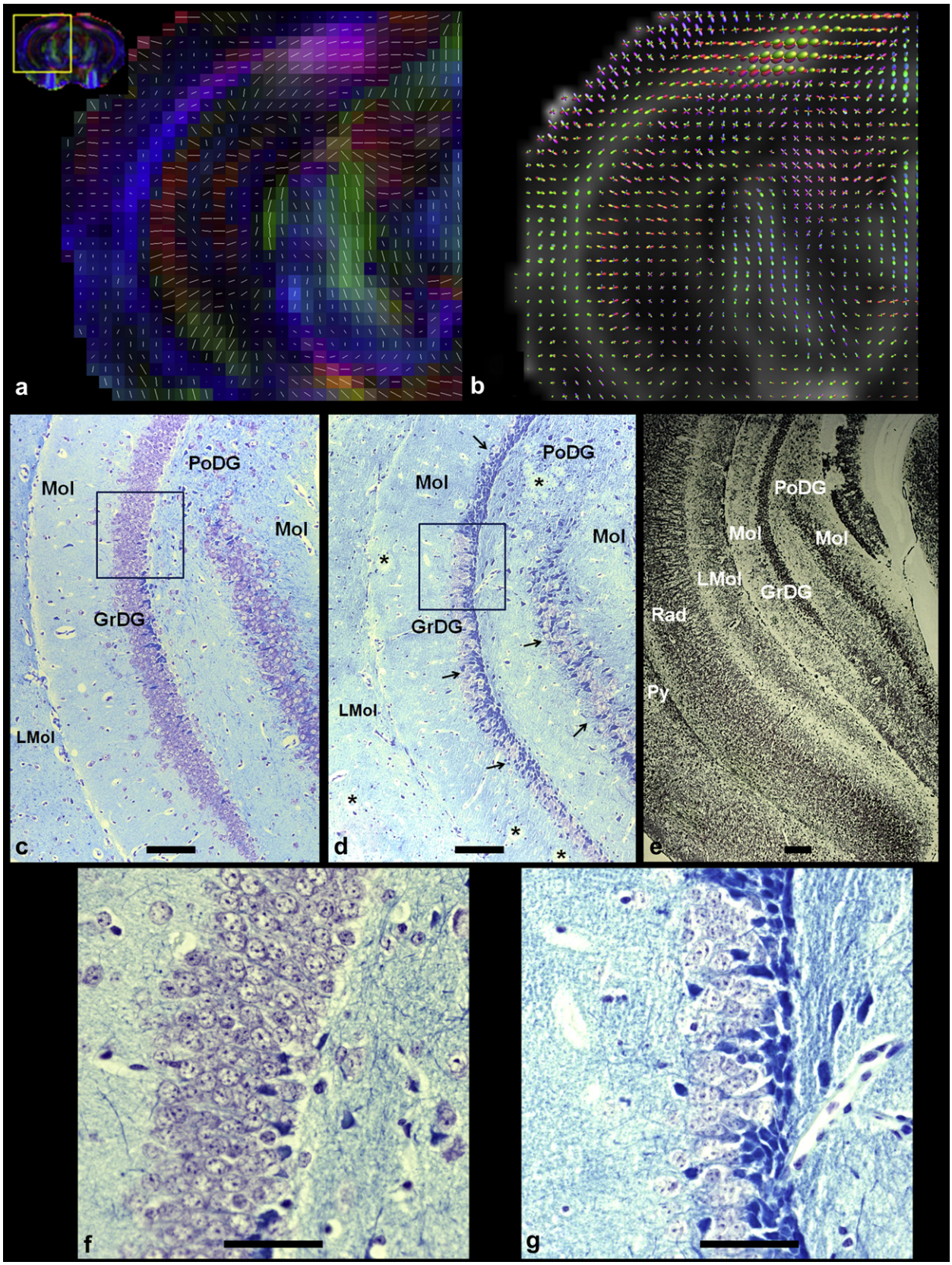

Fig. 4. Diffusion orientations in a representative wild type (WT) mouse hippocampus at 12 months of age (a, b). The primary diffusion tensor orientation is overlaid on fractional anisotropy (FA) maps, color-coded by the diffusion orientation (a). The diffusion is shown with fiber orientation distribution (FODs) overlaid on the FA (b). In the hippocampus, 2 layers of marked anisotropy and medial-lateral orientation alternate with 2 layers of more isotropic diffusion. The anatomic orientation of the axons is visualized in the hippocampal layers by the Klüver-Barrera staining in a WT and an $APP_{swe}/PS1_{dE9}$ mouse (c and d respectively, 10× magnification) and in a WT mouse by Bodian staining (e, 5× magnification). In the stratum radiatum (Rad) and in the molecular layer of the dentate gyrus (Mol) the fibers are oriented in the direction radial to the cortical surface, as

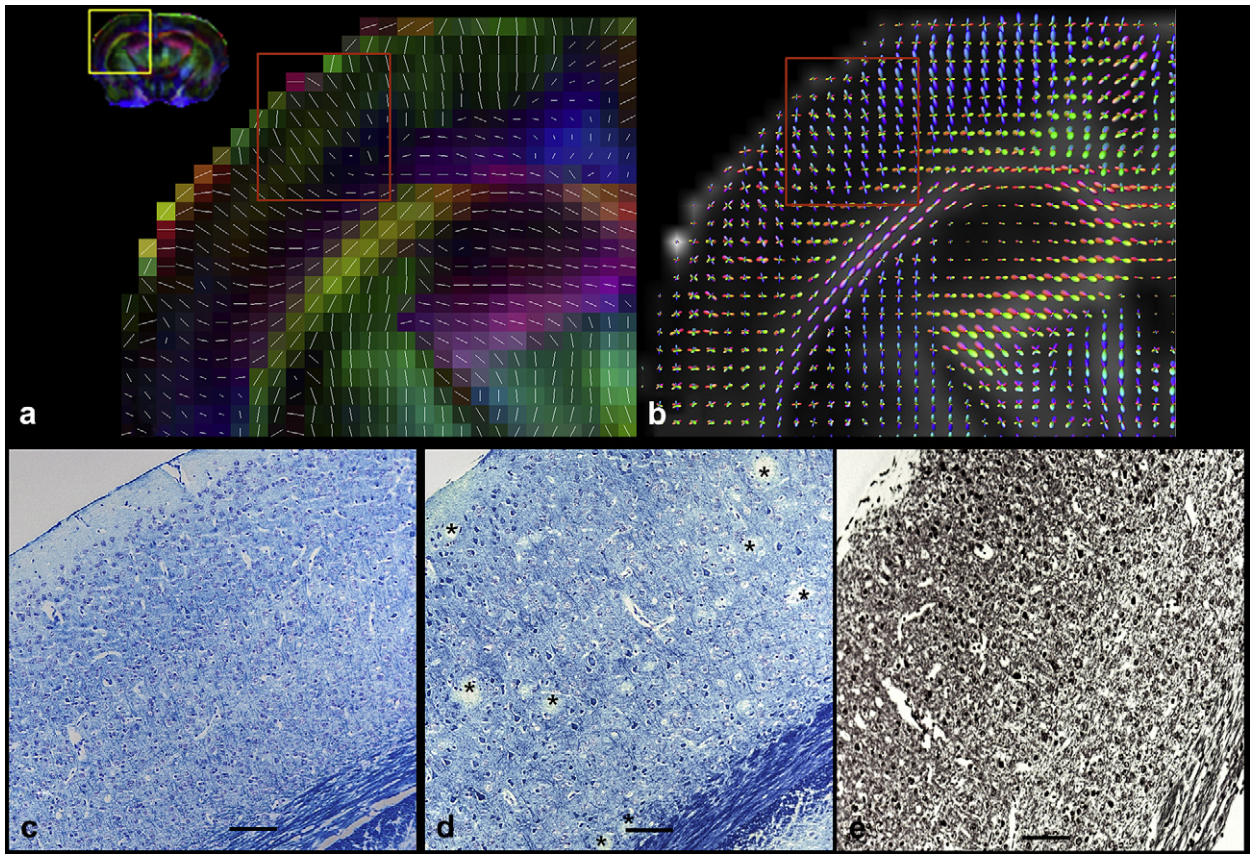

Fig. 5. Diffusion orientations in a representative mouse brain cortex at 12 months of age (a and b). The primary diffusion direction is overlaid on color-coded fractional anisotropy (FA) maps (a). The diffusion is shown with fiber orientation distributions overlaid on the FA (b). The diffusion direction well resembles the actual axonal orientation radial to the cortical surface, as shown with the Klüver-Barrera staining of a wild type (WT) and an $APP_{swe}/PS1_{dE9}$ mouse (c and d, respectively) and with the Bodian staining of a WT (e) in the same areas (boxes in a and b). The Klüver-Barrera staining of a $APP_{swe}/PS1_{dE9}$ mouse (d) revealed the presence of spherical-shaped areas characterized by omission of staining, where no fibers and cell bodies are present likely because of amyloid-beta plaque deposits in the transgenic animals (d, asterisks). (c, d, and e) Magnification = 10×. Scale bar = 250 μm.

still controversial, this explanation for our results is supported by histologic analysis. In the Klüver-Barrera staining for myelin and nerve cells, we showed clear evidence of neuronal loss with thinning of the whole GrDG layer of the hippocampus in $APP_{swe}/PS1_{dE9}$ mice compared with the WT. Interestingly, the neurodegeneration seems to occur adjacently to the Mol layer of the dentate gyrus (DG), where we demonstrated higher MD in $APP_{swe}/PS1_{dE9}$ mice with DT-MRI.

Similar findings have been found in other studies in APP/PS1 double transgenic mice. Two studies reported a substantial age-related neuronal loss in the hippocampal pyramidal cell layer of APP/PS1 mice that could relate to our results (Ramos et al., 2006; Schmitz et al., 2004). Lower levels of glucose uptake were measured with fluoro-d-glucose positron emission tomography in APP/PS1 mice compared with PS1 mice in the LMol and in the stratum radiatum of the hippocampus (Dubois et al., 2010). Moreover, in 12-month-old $APP_{swe}/PS1_{dE9}$ mice, robust axonal loss (approximately 50%) of monoaminergic neurons in hippocampal and cortical regions was observed, which was correlated with progressive atrophy of cell bodies and loss of monoaminergic neurons (Liu et al., 2008).

Vascular alterations are closely associated with amyloid angiopathy, and could contribute to a progressive neuronal loss because of chronic hypoperfusion and/or ischemia (de la Torre, 2002). Many reports, including some from our group, described a reduction in cerebral blood volume in the hippocampus of APP/PS1 mice (Hooijmans et al., 2009; Wu et al., 2004; Zerbi et al., 2012). Furthermore, several changes in behavior and memory impairment are known in these mice, and suggest hippocampal neuronal malfunction or loss (Hooijmans et al., 2009). The histologic staining methods did not reveal neuronal loss in the cerebral cortex of $APP_{swe}/PS1_{dE9}$ mice. However in this area, the absence of staining of neurons and nerve fibers in the spherically shaped areas is likely because of a severe cortical Aβ plaque load. The presence of Aβ plaques might result in a more isotropic diffusion on the voxel level, because the structure of the Aβ is unlikely to contribute to anisotropy. This is in agreement with the reduction in cortical FA in our DT-MRI results for the $APP_{swe}/PS1_{dE9}$ mice compared with WT.

visible in the Bodian staining (e). A less coherent alignment of the nerve fibers is found instead in the lacunosum moleculare layer (LMol), in the granulate layer of the dentate gyrus (GrDG), and in the polymorph layer of the dentate gyrus (PoDG). Overall, a good anatomic agreement is found between diffusion data and nerve fibers directionality and alignment. The Klüver-Barrera staining of a WT (c) and of an $APP_{swe}/PS1_{dE9}$ (d) and their correspondent magnifications (f, and g, 40× magnification) illustrate neurodegeneration in the transgenic mice, with thinner GrDG layer (d, arrows), loss of healthy neurons and many pycnotic dark stained cells and spherical-shaped areas with no staining, possibly because of the presence of amyloid-beta plaques (d, asterisks). diffusion tensor magnetic resonance images and staining sections were selected at bregma −2.92 mm, based on the atlas of Franklin and Paxinos (1997). (c, d, and e) Scale bar = 250 μm; (f and g) scale bar = 50 μm.

4.3. Methodological considerations

For achieving fast and high-resolution echo planar images with a good signal-to-noise ratio, the use of ultra-high field magnet strength coupled with powerful gradients and highly sensitive radiofrequency coils are prerequisites. Especially at ultra-high field (>7 T), susceptibility inhomogeneities that can cause image distortion must be properly adjusted by careful shimming. Furthermore, respiration and head movement must be avoided during the acquisition (e.g., by using a stereotactic holder) and should be further corrected with postprocessing methods (Zwiers, 2010). All these criteria were fulfilled in this study.

The advantages in signal-to-noise ratio allowed us to acquire high spatial resolution data in a short acquisition time. The use of high resolution is necessary to describe diffusion proprieties in small brain structures, and is particularly important to reduce the partial volume effect in structures neighboring cerebrospinal fluid (CSF) or at the interface between gray and white matter. In these areas, the presence of different structures in 1 voxel can bring about an erroneous evaluation of DT-MRI parameters. In AD patients with brain atrophy the enlargement of cerebral ventricles might contribute to an increased MD (Kwong et al., 1991). An increase of the CSF area has also been observed in APP/PS1 mice by high-resolution MRI volumetry (Delatour et al., 2006). From our VBA, we detected an increase in MD and RD and a decrease in FA in voxels along the hippocampal CA3 region and left and right ventricles. It is possible that the increase in ventricle size and atrophy of the fimbria of the hippocampus might have influenced these results, because of partial volume effects. The anatomic differences between groups and the influence of image deformation was however reduced by the use of a study-specific template and by the nonlinear diffeomorphic transformation applied for the spatial normalization of the individual datasets. This makes it unlikely that partial volume effects near CSF areas have influenced the results in the hippocampal subregions.

In conclusion, in this report we describe a method to acquire and process high-resolution DT-MRI images in mice with a voxel-based approach. This method was applied to evaluate changes in water diffusivity in white and gray matter occurring in 12-month-old $APP_{swe}/PS1_{dE9}$ mice, with a spatial characterization of the effects not limited to predetermined neuroanatomic locations. Because changes in DT-MRI parameters have been associated with progression in neuronal and myelin damage, the method and results presented here provide the basis for further studies on the biological cause of diffusion changes and for evaluation of the efficiency of future treatment strategies in mice models for AD and other neurodegenerative disorders.

Disclosure statement

All authors have no conflict of interest to declare.

The experiments were performed according to Dutch federal regulations for animal protection and were approved by the Veterinary Authority of the Radboud University Nijmegen Medical Centre.

Acknowledgements

The authors thank Henk Arnts and Bianca Lemmers for taking care of the mice, and Dr Marcel P. Zwiers for his scientific support in using the PATCH algorithm.

The research leading to these results has received funding from the EU FP7 project LipiDiDiet, Grant Agreement 211696, and was supported by NWO investment grants 91106021 and BIG (VISTA).

References

Arnold, S.E., Hyman, B.T., Flory, J., Damasio, A.R., Van Hoesen, G.W., 1991. The topographical and neuroanatomical distribution of neurofibrillary tangles and neuritic plaques in the cerebral cortex of patients with Alzheimer's disease. Cereb. Cortex 1, 103–116.

Avants, B., Duda, J.T., Kim, J., Zhang, H., Pluta, J., Gee, J.C., Whyte, J., 2008. Multivariate analysis of structural and diffusion imaging in traumatic brain injury. Acad Radiol. 15 (11), 1360–1375.

Basser, P.J., Mattiello, J., LeBihan, D., 1994. MR diffusion tensor spectroscopy and imaging. Biophys. J. 66, 259–267.

Beaulieu, C., 2002. The basis of anisotropic water diffusion in the nervous system - a technical review. NMR Biomed. 15, 435–455.

Bodian, David., 1936. A new method for staining nerve fibers and nerve endings in mounted paraffin sections. Anat. Rec. 65, 89–97.

Bodian, David., 1937. The staining of paraffin sections of nervous tissues with activated protargol. The role of fixatives Anat. Rec. 69, 153–162.

Bozzali, M., Falini, A., Franceschi, M., Cercignani, M., Zuffi, M., Scotti, G., Comi, G., Filippi, M., 2002. White matter damage in Alzheimer's disease assessed in vivo using diffusion tensor magnetic resonance imaging. J. Neurol. Neurosurg. Psychiatry 72, 742–746.

Braak, H., Braak, E., 1991. Neuropathological stageing of Alzheimer-related changes. Acta Neuropathol. 82, 239–259.

Braak, H., Braak, E., 1995. Staging of Alzheimer's disease-related neurofibrillary changes. Neurobiol. Aging 16, 271–278; discussion 278–284.

Bronge, L., Bogdanovic, N., Wahlund, L.O., 2002. Postmortem MRI and histopathology of white matter changes in Alzheimer brains. A quantitative, comparative study. Dement. Geriatr. Cogn. Disord. 13, 205–212.

Budde, M.D., Frank, J.A., 2012. Examining brain microstructure using structure tensor analysis of histological sections. Neuroimage 63, 1–10.

Carlesimo, G.A., Cherubini, A., Caltagirone, C., Spalletta, G., 2010. Hippocampal mean diffusivity and memory in healthy elderly individuals: a cross-sectional study. Neurology 74, 194–200.

Chen, H., Epelbaum, S., Delatour, B., 2011. Fiber tracts anomalies in APPxPS1 transgenic mice modeling Alzheimer's disease. J. Aging Res. 2011, 281274.

de Groot, J.C., de Leeuw, F.E., Oudkerk, M., van Gijn, J., Hofman, A., Jolles, J., Breteler, M.M., 2000. Cerebral white matter lesions and cognitive function: the Rotterdam Scan Study. Ann. Neurol. 47, 145–151.

de la Torre, J.C., 2002. Alzheimer disease as a vascular disorder: nosological evidence. Stroke 33, 1152–1162.

Delatour, B., Guegan, M., Volk, A., Dhenain, M., 2006. In vivo MRI and histological evaluation of brain atrophy in APP/PS1 transgenic mice. Neurobiol. Aging 27, 835–847.

Di Paola, M., Di Iulio, F., Cherubini, A., Blundo, C., Casini, A.R., Sancesario, G., Passafiume, D., Caltagirone, C., Spalletta, G., 2010. When, where, and how the corpus callosum changes in MCI and AD: a multimodal MRI study. Neurology 74, 1136–1142.

Douaud, G., Jbabdi, S., Behrens, T.E., Menke, R.A., Gass, A., Monsch, A.U., Rao, A., Whitcher, B., Kindlmann, G., Matthews, P.M., Smith, S., 2011. DTI measures in crossing-fibre areas: increased diffusion anisotropy reveals early white matter alteration in MCI and mild Alzheimer's disease. Neuroimage 55, 880–890.

Dubois, A., Herard, A.S., Delatour, B., Hantraye, P., Bonvento, G., Dhenain, M., Delzescaux, T., 2010. Detection by voxel-wise statistical analysis of significant changes in regional cerebral glucose uptake in an APP/PS1 transgenic mouse model of Alzheimer's disease. Neuroimage 51, 586–598.

Dubois, A., Herard, A.S., Flandin, G., Duchesnay, E., Besret, L., Frouin, V., Hantraye, P., Bonvento, G., Delzescaux, T., 2008. Quantitative validation of voxel-wise statistical analyses of autoradiographic rat brain volumes: application to unilateral visual stimulation. Neuroimage 40, 482–494.

Englund, E., 1998. Neuropathology of white matter changes in Alzheimer's disease and vascular dementia. Dement. Geriatr. Cogn. Disord. 9 (suppl 1), 6–12.

Englund, E., Brun, A., 1990. White matter changes in dementia of Alzheimer's type: the difference in vulnerability between cell compartments. Histopathology 16, 433–439.

Fellgiebel, A., Wille, P., Muller, M.J., Winterer, G., Scheurich, A., Vucurevic, G., Schmidt, L.G., Stoeter, P., 2004. Ultrastructural hippocampal and white matter alterations in mild cognitive impairment: a diffusion tensor imaging study. Dement. Geriatr. Cogn. Disord. 18, 101–108.

Fellgiebel, A., Dellani, P.R., Greverus, D., Scheurich, A., Stoeter, P., Muller, M.J., 2006. Predicting conversion to dementia in mild cognitive impairment by volumetric and diffusivity measurements of the hippocampus. Psychiatry Res. 146, 283–287.

Franklin, K.B.J., Paxinos, G., 1997. The Mouse Brain in Stereotaxic Coordinates. Academic Press, San Diego.

Garcia-Alloza, M., Robbins, E.M., Zhang-Nunes, S.X., Purcell, S.M., Betensky, R.A., Raju, S., Prada, C., Greenberg, S.M., Bacskai, B.J., Frosch, M.P., 2006. Characterization of amyloid deposition in the APPswe/PS1dE9 mouse model of Alzheimer disease. Neurobiol. Dis. 24, 516–524.

Hanyu, H., Sakurai, H., Iwamoto, T., Takasaki, M., Shindo, H., Abe, K., 1998. Diffusion-weighted MR imaging of the hippocampus and temporal white matter in Alzheimer's disease. J. Neurol. Sci. 156, 195–200.

Harms, M.P., Kotyk, J.J., Merchant, K.M., 2006. Evaluation of white matter integrity in ex vivo brains of amyloid plaque-bearing APPsw transgenic mice using magnetic resonance diffusion tensor imaging. Exp. Neurol. 199, 408–415.

Harsan, L.A., Paul, D., Schnell, S., Kreher, B.W., Hennig, J., Staiger, J.F., von Elverfeldt, D., 2010. In vivo diffusion tensor magnetic resonance imaging and fiber tracking of the mouse brain. NMR Biomed. 23, 884–896.

Hooijmans, C.R., Van der Zee, C.E., Dederen, P.J., Brouwer, K.M., Reijmer, Y.D., van Groen, T., Broersen, L.M., Lutjohann, D., Heerschap, A., Kiliaan, A.J., 2009. DHA and cholesterol containing diets influence Alzheimer-like pathology, cognition and cerebral vasculature in APPswe/PS1dE9 mice. Neurobiol. Dis. 33, 482–498.

Jankowsky, J.L., Slunt, H.H., Ratovitski, T., Jenkins, N.A., Copeland, N.G., Borchelt, D.R., 2001. Co-expression of multiple transgenes in mouse CNS: a comparison of strategies. Biomol. Eng. 17, 157–165.

Jankowsky, J.L., Slunt, H.H., Gonzales, V., Jenkins, N.A., Copeland, N.G., Borchelt, D.R., 2004. APP processing and amyloid deposition in mice haplo-insufficient for presenilin 1. Neurobiol. Aging 25, 885–892.

Jiang, Y., Johnson, G.A., 2010. Microscopic diffusion tensor imaging of the mouse brain. Neuroimage 50, 465–471.

Kantarci, K., 2011. Diffusion tensor imaging in Alzheimer's disease. Curr. Med. Imaging Rev. 7, 6.

Kantarci, K., Petersen, R.C., Boeve, B.F., Knopman, D.S., Weigand, S.D., O'Brien, P.C., Shiung, M.M., Smith, G.E., Ivnik, R.J., Tangalos, E.G., Jack Jr., C.R., 2005. DWI predicts future progression to Alzheimer disease in amnestic mild cognitive impairment. Neurology 64, 902–904.

Klüver, H., Barrera, E., 1953. A method for the combined staining of cells and fibers in the Nervous system. J. Nueropath. Exp. Neurol. 12, 400–403.

Kwong, K.K., McKinstry, R.C., Chien, D., Crawley, A.P., Pearlman, J.D., Rosen, B.R., 1991. CSF-suppressed quantitative single-shot diffusion imaging. Magn. Reson. Med. 21, 157–163.

Le Bihan, D., Breton, E., Lallemand, D., Grenier, P., Cabanis, E., Laval-Jeantet, M., 1986. MR imaging of intravoxel incoherent motions: application to diffusion and perfusion in neurologic disorders. Radiology 161, 401–407.

Liu, Y., Yoo, M.J., Savonenko, A., Stirling, W., Price, D.L., Borchelt, D.R., Mamounas, L., Lyons, W.E., Blue, M.E., Lee, M.K., 2008. Amyloid pathology is associated with progressive monoaminergic neurodegeneration in a transgenic mouse model of Alzheimer's disease. J Neurosci 17;28 (51), 13805–13814. http://dx.doi.org/10.1523/JNEUROSCI.4218-08.2008.

Malm, T., Koistinaho, J., Kanninen, K., 2011. Utilization of APPswe/PS1dE9 transgenic mice in research of Alzheimer's disease: focus on gene therapy and cell-based therapy applications. Int. J. Alzheimers Dis. 2011, 517160.

Medina, D., DeToledo-Morrell, L., Urresta, F., Gabrieli, J.D., Moseley, M., Fleischman, D., Bennett, D.A., Leurgans, S., Turner, D.A., Stebbins, G.T., 2006. White matter changes in mild cognitive impairment and AD: a diffusion tensor imaging study. Neurobiol. Aging 27, 663–672.

Mueggler, T., Meyer-Luehmann, M., Rausch, M., Staufenbiel, M., Jucker, M., Rudin, M., 2004. Restricted diffusion in the brain of transgenic mice with cerebral amyloidosis. Eur. J. Neurosci. 20, 811–817.

Ramos, B., Baglietto-Vargas, D., del Rio, J.C., Moreno-Gonzalez, I., Santa-Maria, C., Jimenez, S., Caballero, C., Lopez-Tellez, J.F., Khan, Z.U., Ruano, D., Gutierrez, A., Vitorica, J., 2006. Early neuropathology of somatostatin/NPY GABAergic cells in the hippocampus of a PS1xAPP transgenic model of Alzheimer's disease. Neurobiol. Aging 27, 1658–1672.

Ruest, T., Holmes, W.M., Barrie, J.A., Griffiths, I.R., Anderson, T.J., Dewar, D., Edgar, J.M., 2011. High-resolution diffusion tensor imaging of fixed brain in a mouse model of Oelizaeus-Merzbacher disease: comparison with quantative measores of white matter pathology. NMR Biomed. 24, 1369–1379.

Sawiak, S.J., Wood, N.I., Williams, G.B., Morton, A.J., Carpenter, T.A., 2009. Voxel-based morphometry in the R6/2 transgenic mouse reveals differences between genotypes not seen with manual 2D morphometry. Neurobiol. Dis. 33, 20–27.

Schmitz, C., Rutten, B.P., Pielen, A., Schafer, S., Wirths, O., Tremp, G., Czech, C., Blanchard, V., Multhaup, G., Rezaie, P., Korr, H., Steinbusch, H.W., Pradier, L., Bayer, T.A., 2004. Hippocampal neuron loss exceeds amyloid plaque load in a transgenic mouse model of Alzheimer's disease. Am. J. Pathol. 164, 1495–1502.

Song, S.K., Kim, J.H., Lin, S.J., Brendza, R.P., Holtzman, D.M., 2004. Diffusion tensor imaging detects age-dependent white matter changes in a transgenic mouse model with amyloid deposition. Neurobiol. Dis. 15, 640–647.

Song, S.K., Yoshino, J., Le, T.Q., Lin, S.J., Sun, S.W., Cross, A.H., Armstrong, R.C., 2005. Demyelination increases radial diffusivity in corpus callosum of mouse brain. Neuroimage 26, 132–140.

Sun, S.W., Liang, H.F., Cross, A.H., Song, S.K., 2008. Evolving Wallerian degeneration after transient retinal ischemia in mice characterized by diffusion tensor imaging. Neuroimage 40, 1–10.

Sun, S.W., Song, S.K., Harms, M.P., Lin, S.J., Holtzman, D.M., Merchant, K.M., Kotyk, J.J., 2005. Detection of age-dependent brain injury in a mouse model of brain amyloidosis associated with Alzheimer's disease using magnetic resonance diffusion tensor imaging. Exp. Neurol. 191, 77–85.

Sykova, E., Vorisek, I., Antonova, T., Mazel, T., Meyer-Luehmann, M., Jucker, M., Hajek, M., Ort, M., Bures, J., 2005. Changes in extracellular space size and geometry in APP23 transgenic mice: a model of Alzheimer's disease. Proc. Natl. Acad. Sci. U. S. A. 102, 479–484.

Teipel, S.J., Bayer, W., Alexander, G.E., Zebuhr, Y., Teichberg, D., Kulic, L., Schapiro, M.B., Moller, H.J., Rapoport, S.I., Hampel, H., 2002. Progression of corpus callosum atrophy in Alzheimer disease. Arch. Neurol. 59, 243–248.

Tomimoto, H., Lin, J.X., Matsuo, A., Ihara, M., Ohtani, R., Shibata, M., Miki, Y., Shibasaki, H., 2004. Different mechanisms of corpus callosum atrophy in Alzheimer's disease and vascular dementia. J. Neurol. 251, 398–406.

Tournier, J.D., Calamante, F., Connelly, A., 2007. Robust determination of the fibre orientation distribution in diffusion MRI: non-negativity constrained super-resolved spherical deconvolution. Neuroimage 35, 1459–1472.

Wu, E.X., Tang, H., Asai, T., Yan, S.D., 2004. Regional cerebral blood volume reduction in transgenic mutant APP (V717F, K670N/M671L) mice. Neurosci. Lett. 365, 223–227.

Xie, S., Xiao, J.X., Gong, G.L., Zang, Y.F., Wang, Y.H., Wu, H.K., Jiang, X.X., 2006. Voxel-based detection of white matter abnormalities in mild Alzheimer disease. Neurology 66, 1845–1849.

Zerbi, V., Jansen, D., Dederen, P.J., Veltien, A., Hamans, B., Liu, Y., Heerschap, A., Kiliaan, A.J., 2012. Microvascular cerebral blood volume changes in aging APP(swe)/PS1 (dE9) AD mouse model: a voxel-wise approach. Brain Struct. Funct. http://dx.doi.org/10.1007/s00429-012-0448-8

Zwiers, M.P., 2010. Patching cardiac and head motion artefacts in diffusion-weighted images. Neuroimage 53, 565–575.